Journal of Multidisciplinary Engineering Science and Technology (JMEST)
ISSN: 2458-9403
Vol. 7 Issue 6, June - 2020

Design And Construction Of Circuits For An Integrated Solar-Wind Energy System With Remote Monitoring And Control Mechanism

Usah, Emmamuel Okon[1]
Department of Physics
University of Uyo

Ozuomba, Simeon[2]
Department of Electrical/Electronic and Computer Engineering
University of Uyo
simeonozuomba@uniuyo.edu.ng
simeonoz@yahoo.com

Etinamabasiyaka Edet Ekott[3]
Department of Physics
University of Uyo

***Abstract*— In this paper, the design and construction of the circuits for an integrated solar-wind energy system with remote monitoring and control mechanism is presented. The system block diagram was developed and it has six major sub-sections, namely, the solar/wind charge controller section, the inverter section, the grid connection section, the rectification section, the onboard/remote monitoring control section and the energy storage section. In addition, each sub-section is also made up of sub-units which provide detailed information on the components used. The circuit diagram for the sub-units were presented along with numerical examples of calculations used to determine some circuit components values. Also, the implementation of project was carried out in sub-sections, particularly; the various sub-sections were constructed and assemble using Vero board. The circuits were simulated using Proteus software and the output signals of some parts of the circuits were presented. Also, the implemented circuits were tested and the test results show that the implemented circuits operate in line with the design specification.**

Keywords*— Integrated Solar-Wind Energy, Photovoltaic Power, Wind Turbine, Android Application, Remote Monitoring System, Proteus Software

1. Introduction

Generally, the availability of hybrid renewable energy sources is growing rapidly in many developed and developing countries [1,2,3,4,5,6]. Growth in two common renewable energy sources , namely, wind and photovoltaic (PV) has been so significant in recent years [7,8,9,10,11,12]. Moreover, the high growth rates are expected to continue for renewable technologies for several years to come. One or the reason is because wind and photovoltaic (PV) are environmentally friendly power sources and the basis for most renewable energy development policies is the growing demand for environmentally power solutions [13,14,15,16,17,18]. An integrated renewable energy system includes renewable energy generation, energy storage and certain transmission components [19,20,21,22,23]. A renewable energy system is sustainable unlike the fossil fuel sources that deplete with use [24,25,26]. As such, the use of modern hybrid renewable energy technologies, including wind/solar panels, solar energy/ biomass pellets, small hydro/solar etc, continues to increase rapidly. However, based on the findings so far among different types of renewable energy sources, system for integration of solar and wind sources is considered in this work as it will go a long way in solving today and future energy crisis.

Basically, this work is all about the development of circuits for an integrated solar- wind energy system with remote monitoring and control mechanism is presented. The system is capable of receiving two sources of power supply, that is from solar, wind energy and harmonize the energies into a single ac voltage power supply. The system is designed and equipped with various sensors and protective sub-systems as well as a two ways communication system. In this work, several protective sub-systems and sensors are introduced so as to protect and control the input and output parameters.

2. Methodology

The focus of this paper is on the system block diagram, the system operation, the circuit design, analysis and implementation for an integrated solar-wind energy system with remote monitoring and control mechanism.

2.1 The System block diagram and the description of the System

The block diagram of the integrated solar-wind energy system is shown in Figure 1. According to Figure 1, the system block diagram is divided into six major sub-sections, namely, the solar/wind charge controller section, the inverter section, the grid connection section, the rectification section, the onboard/remote monitoring control section and the energy storage section. However, each sub-section is also made up of sub-units which provide detailed information on the components used. The section marked with red dotted line in Figure 1 indicates the solar/wind charge controller section, which is made up of four units, namely; the solar input unit, the wind input unit, the solar charge controller unit and the wind charge controller unit. Similarly, the inverter section denoted with blue dotted lines has four units, which are the relay switch 1 unit, the multi-vibrator unit, the drivers unit, the step-up transformer unit and relay unit. The grid connection section shown in purple lines consists of two units, which includes the grid input and high/low grid voltage control units. Again, the

rectifier/filter unit and the relay switch 2 constitute the rectification section which is delineated with brown dotted lines. The green lines indicate the onboard/remote monitoring control section, which has only three units. These are the microcontroller unit, the GSM/GPRS unit and the display unit. The energy storage section has only one unit which is the battery bank.

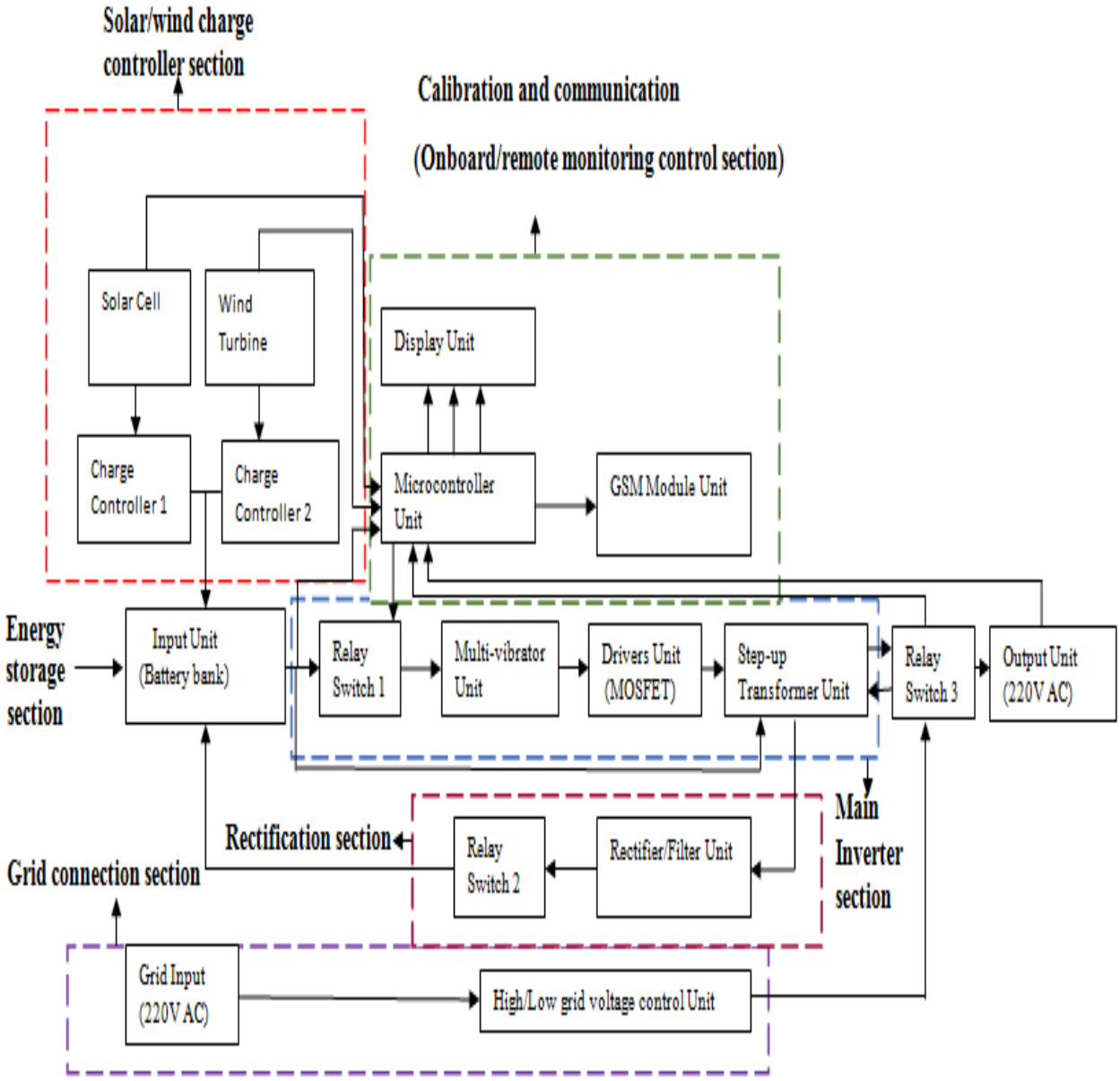

Figure 1: Block diagram of Smart Modular Integrated Solar and Wind Energy System

Basically, the system operates in two modes; the inverter mode or un-interrupted power supply mode (UPS) and the non-inverter mode. During the inverter mode (i.e solar/wind charge controller section), the energy captured from the two sources (solar panel and wind turbine) are synchronized and stored in the battery bank unit. The stored energy releases the electrical energy to the inverter main section, where the relay switch 1 unit is used to engage the multi-vibrator unit. The multi-vibrator unit then generates an astable pulse or free running pulse (square wave) which is used to feed the driver's unit. At this point, the driver unit uses the low ac voltage (12Vac) to drive the primary coil of the step-up transformer and 220Vac is obtained across the secondary of the transformer which is the output unit.

However, whenever there is grid power, the system switches automatically over from the inverter mode (UPS) to the non-inverter mode. In operation, the system is supplying the load and also charging the battery bank as indicated in the block diagram of Figure 3.1. During the non-inverter mode, beginning from the grid connection section (i.e 220Vac input), the AC signal is allowed to passed through the high/low voltage control unit so as to allow a nominal voltage to pass to the system. Here, a certain range of high and low voltage is allowed through the control unit. Specifically, in this research, 180V is viewed as the minimum voltage in the range, while 220V is viewed as the maximum voltage in the range. At this point, when the required voltage range reaches relay switch 3, the voltage is shared into two. One flows to the output

unit (load), while the other flows into the rectification section from the step-up transformer which also serves as a step-down transformer during the non-inverter mode. The grid voltage is then rectified and filtered before it is allowed to pass through relay switch 2 to the battery bank for charging of the batteries. The relay switch 2 is used to cut-off the charging voltage at a certain reference point when the battery is fully charged.

Furthermore, to communicate between the system and the user, an onboard/remote monitoring section is introduced, where the microcontroller unit is employed. Among other functions, the microcontroller unit monitors the charging process during the non-inverter mode, coordinates all information flow in the entire system and displays them on the screen. System information is also process by the microcontroller and sent to the cell phone via the GPRS/GPS module. The information includes the input voltages, the input current, the input power from the solar panel and the wind turbine, the battery voltage, the grid voltage and the system output voltage. The GPRS/GPS module unit transmits the data gathered by microcontroller in the GSM network in the form of packets, where it can be accessed with cell phone from anywhere across the globe.

2.2 The Circuit and Operation of the Main Inverter/Low Battery Voltage Shutdown Circuit

The circuit diagram of the integrated solar and wind energy system is segmented into three major sub-circuits, namely, the inverter/low battery voltage shutdown circuit shown in Figure 2, the charge controller, high/low grid voltage control circuit, shown in Figure 3, as well as the calibration and communication (onboard diagnostic/remote monitoring) circuit, shown in Figure 4.

The circuit diagram of the main inverter/low battery voltage shutdown system is shown in Figure 2. The circuit comprises of seven sub-circuits. The seven sub-circuits are the low battery voltage switch (2N2222), the multi-vibrator (CD4047), the AND gate (4081), the comparator (LM324), the drivers (IRF3205), the transformer (12V/220V) and the rectification unit (bridge rectifier; 1N4007). During system operation, all the units work sequentially based on the designed function.

The first stage of operation is whenever switch S1 is turned on, the low battery sub-circuit controlled by transistor Q5 (2N2222) checks whether the battery potential is up to the required voltage level (i.e 11.5V) and energize the multi-vibrator sub-circuit. The multi-vibrator generates a 50Hz square wave signal via pin 10 and 11 but out of phase to each other.

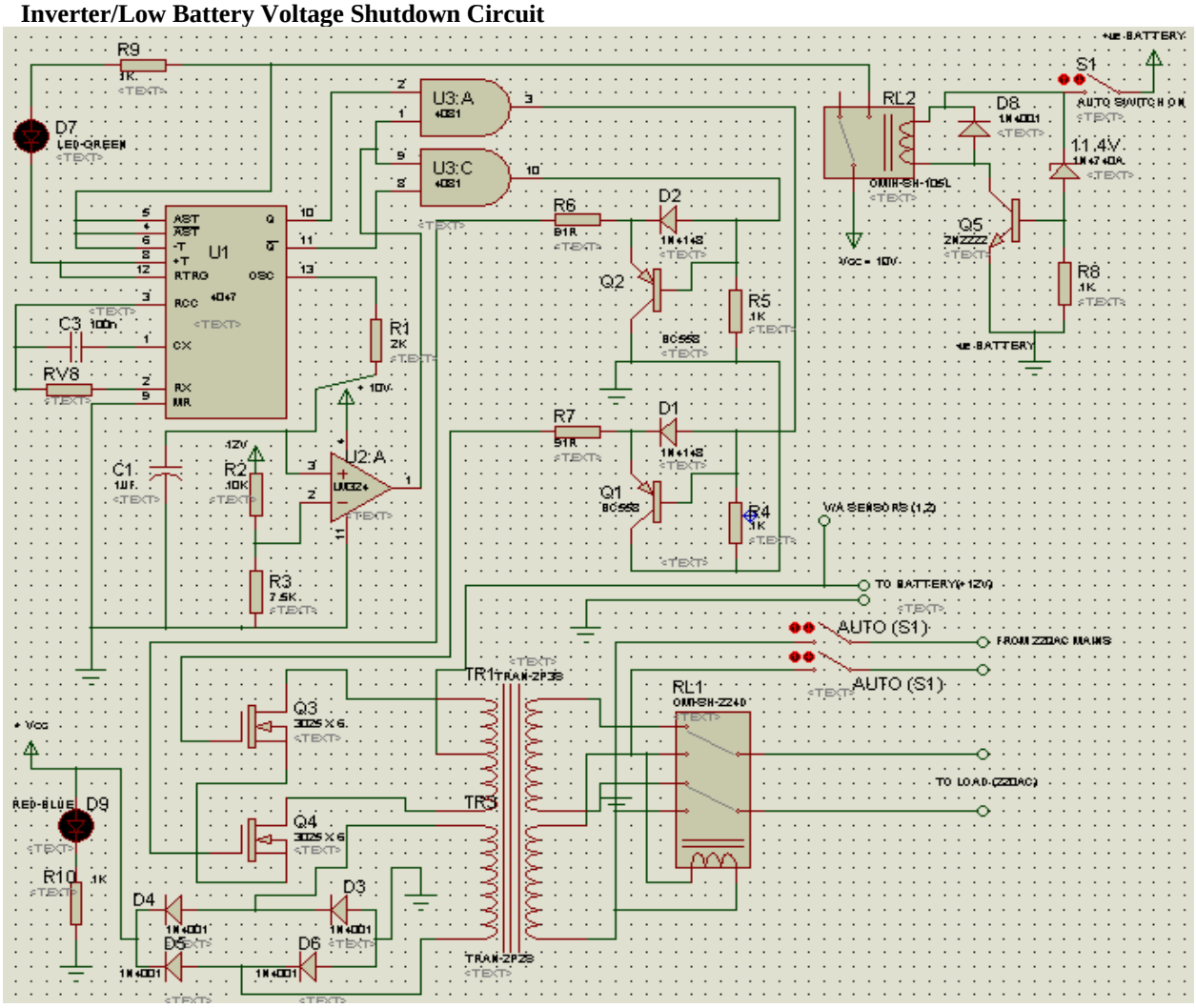

Figure 2: Main Inverter /Low battery voltage shutdown circuit diagram

.

The frequency of the pulse generated at pin 13 is 100Hz, which is twice the frequency of pin 10 and 11, and

all these frequencies are determined by capacitor C3 and resistor RV8. The AND gate (U3:A, U3:C); 4081and comparator LM324 are introduced between the multi-vibrator and the driver (IRF3205) to stabilize the system output especially when the battery voltage begin to drops. The drivers (IRF3205) swing the weak current so as to drive the transformer primary coil to a level where the transformer could be able to step up. At this point, the transformer (TR1) steps up from 12Vac to 220Vac, where it is used to supply the ac loads. However the bridge rectifier configured with diode D3, D4, D5 and D6, is used to charge the battery whenever there is availability of grid power.

2.3 Operation of the Charge Controller and High/Low Grid Voltage control Circuit.

The circuit diagram of charge controller and high/low grid voltage control is as shown in Figure 3. The sub-circuit is made up of few components such as comparator (LM324), MOSFETs (IRF3205), transistor (2N2222), Zener diode (13.2V) and relay switch (12V/400Ω). However, the sub-circuit is made up of two major units, the solar/wind charge controller and the high/low grid control sub-units, the solar/wind sub-unit is responsible for charging battery bank. The high/low grid voltage control unit is to responsible for the maintaining nominal 220Vac voltage, for both charging of the battery bank and powering of the loads when the grid power supply is present.

However, the solar/wind charge controller unit works based on the principle of operation of the MOSFET used. In this case, an NPN transistor (Q7: 2N2222) is used to regulate the source voltage of the N-channel MOSFET Q6. Also, another NPN transistor (Q8: 2N2222) which is biased with a 13.2V zener diode is used to provide a cut-off voltage for the MOSFET switch. In this type of configuration, the drain current is controlled by the source voltage, so that when the input voltage (either solar/wind sources) rises to the zener voltage, the MOSFET drain current is turned off as well as the supply voltage to the battery bank.

On the other hand when there is off-grid power, the high/low grid control sub-unit is activated. It works when the grid input voltage is about 13Vdc, and fed to the two comparators (U2: B, U2: C).In the Comparator U2: B monitors high voltage (220Vac), while U2: C is for low voltage (180). This is done by biasing the two comparators inputs (i.e. inverting and non-inverting inputs) with same the resistor values but different zener voltages. In this case, 6.8Vis for high voltage and 5.5V is for low voltage, respectively. A 1kΩ resistor is used to connect the two comparators outputs together to the base of transistor Q9. The transistor is to help swing the required current to the smooth operation of relay switch RL3. This is where the high/low control sub-unit decides whether to shutdown the inverter mode and supply the load or not. This condition is always determined by the magnitude of the grid input voltage.

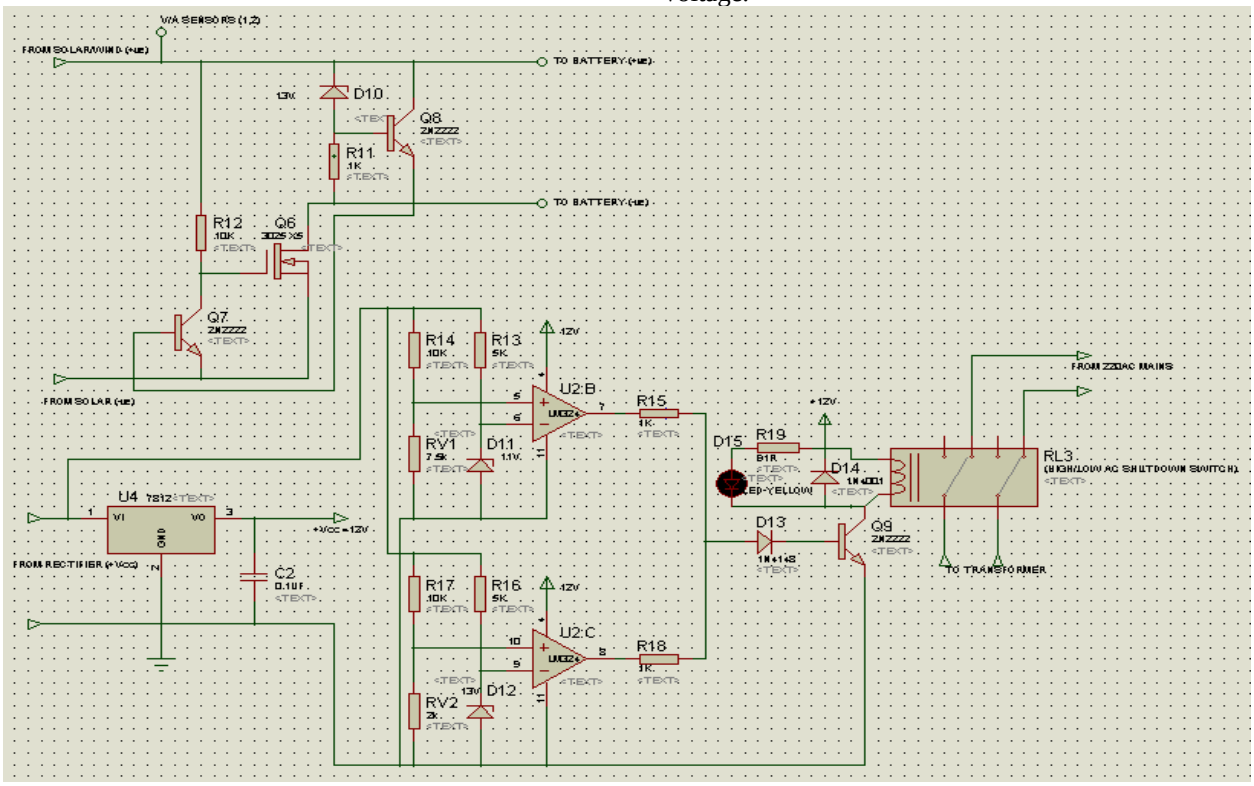

Figure 3: Charge Controller, High/Low Grid Voltage control Circuit Diagram.

2.4 Calibration and Communication (Onboard diagnostic/Remote Monitoring) Circuit Operation

The circuit diagram of calibration and communication (onboard/remote) control system is shown in Figure 4. The circuit is designed with four important components which are current sensors (ACS 712), microcontroller (ATMEGA8L), GSM/GPRS module and voltage regulator (LM317). The system operates by collating, coordinating and collecting all calibrated information (data) from the solar and wind energy sources and sends them to display and GSN/GPRS units. The information (data) is sometimes referred to as solar and wind energy input/output

parameters. They are current (I_{in}, I_{out}), voltages (V_{in}, V_{out}), power (P_{in}, P_{out}), and also included battery bank voltage percentage level.

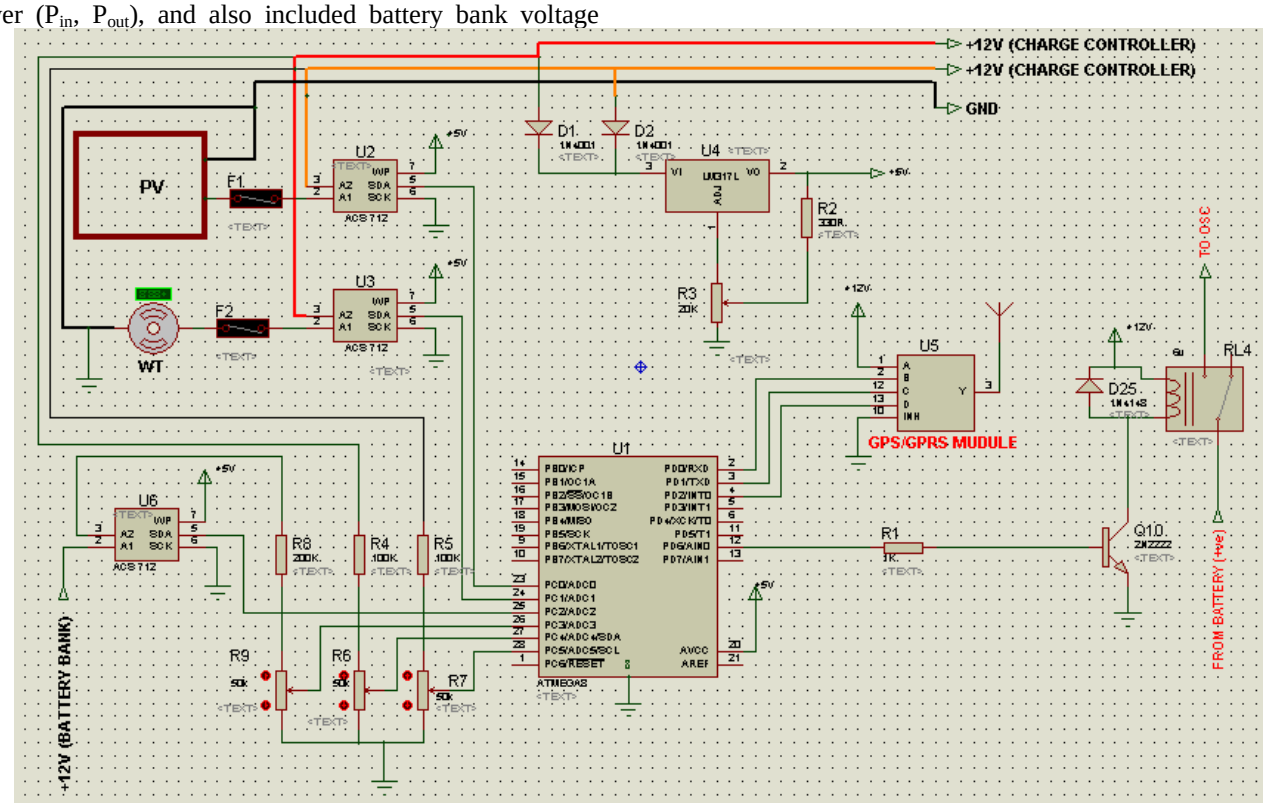

Figure 4: Calibration and communication circuit diagram

However, the circuit is designed such that, when the photovoltaic cell (PV) and wind turbine generates their output voltages and currents, two identical current sensors (ACS 712) are used in-between the solar/wind output and the charge controller to measure their output currents. Here, the input voltages and currents are first measure (calibrated) before allowing them to send to the charge controller. The voltages and currents measured are called open circuit voltages (V_{OC}) and short circuit currents (I_{SC}) respectively. The product of the voltage and current are computed by the microcontroller program and displayed on the cell phone as solar panel output power ($P_{S\ out}$) and wind turbine output power ($P_{W\ out}$). In order to achieve a 5Vdc power supply for the microcontroller and the other units, a voltage regulator is used to normalize the supply voltage from 12Vdc to 5V as shown in the Figure 4.

Furthermore, there is a group of fixed resistor (R4, R5, R8) connected in series with three variable resistors (R6, R7, R9), which are used to regulate voltages and currents to the ADC input pin (Pc2, Pc3, Pc4, Pc5) of the microcontroller. In this work, Pin Pc0 and Pc1 reads the output current of the solar panel and wind turbine respectively. Also Pin Pc2 reads the battery bank level in terms of voltage (% level). In this case, Pin Pc3, Pc4 and Pc5 read the voltage level of the battery, the wind turbine and the solar panel respectively. The microcontroller is programmed such that the output of the microcontroller is obtained across pin (P_{D0}, P_{D1}, P_{D2}). All the three outputs of the microcontroller terminal are coupled to the GSM/GPRS module, so as to enable the system information to be transmitted to the cell phone remotely. However, with the help of cell phone application, information concerning the system can be easily accessed, and can also be switched "ON" or "OFF" at any point in time.

2.5 The Flowchart for the Microcontroller Operation

The operations of the microcontroller section used to manage key operations of the system are summarized in the flowchart of Figure 5.

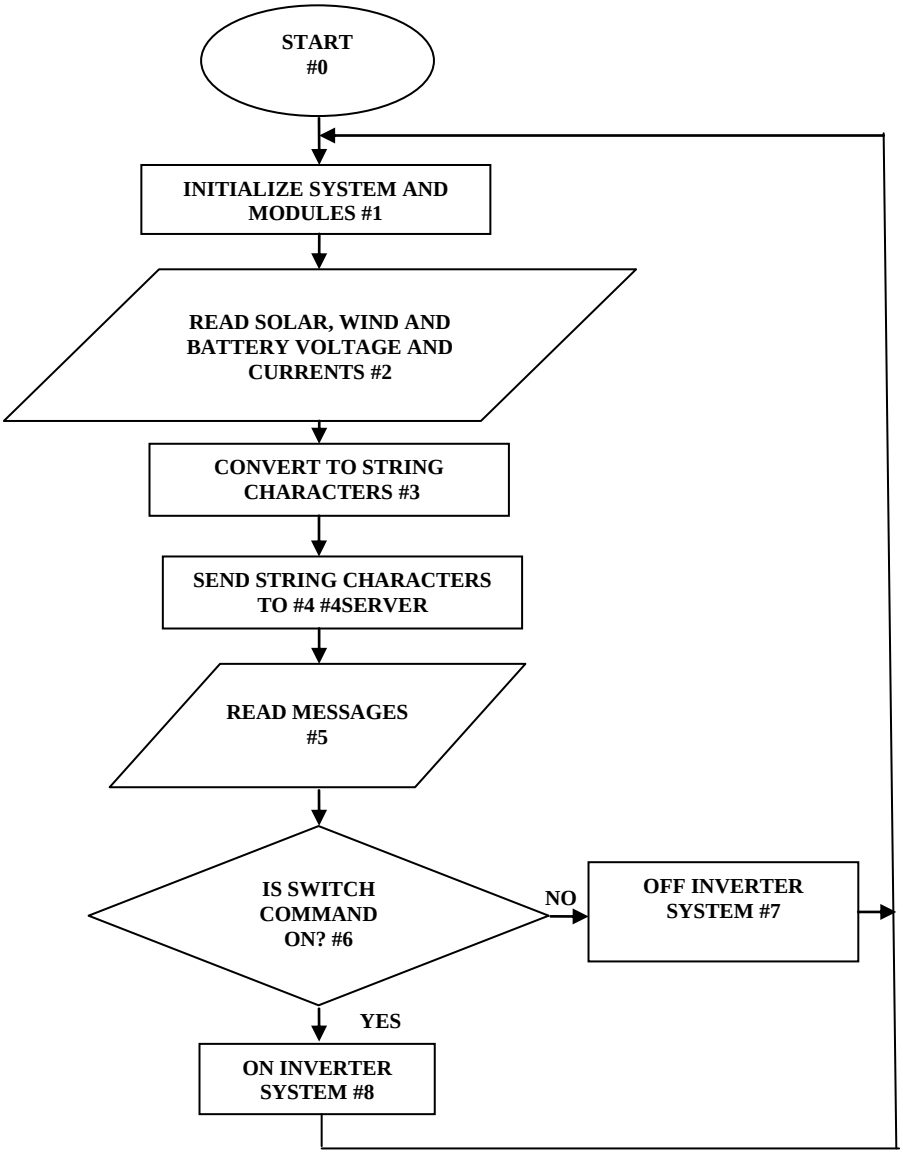

Figure 5: Embedded Program Flowchart

2.6 Circuit analysis

The circuit analysis calculations carried out for some of the major sub-circuits are presented. The calculations are to show how the values, the power ratings, and other parameter values associated with some of the circuit components are determined.

2.6.1 The Analysis of the Transistor Switch Unit

In different sections of the circuits, such as in Figure 4, the 2N2222 NPN transistor is employed as a switch, and it is biased with two resistors, load resistor (RL4) and base (R2). However, the load resistor in Figure 4 is referred to as the resistance of the relay coil (RL4), which is used as a mechanical switch, as shown in Figure 6.

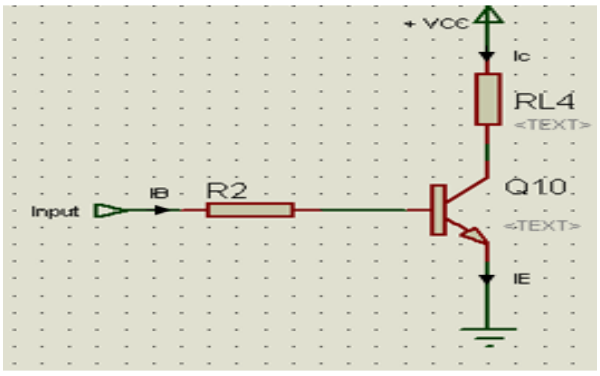

Figure 6: NPN transistor diagram

Also, according to the data book, the following parameter values apply to the 2N2222 transistor: $V_{ce(sat)}$ = V_{be} = 1.0V; I_b = 500mA; H_{fe} = 60 ; Now, consider the cage where V_{in} = 5V, V_{cc} = 12V; $R_c = R_L$ = 100Ω;

The collector current (I_C): The current capable of switching the relay coil (in Figure 6) effectively without causing flapping and arching is computed as follows ;

$$V_{cc} = I_{c(sat)}R_c + V_{cc} \quad (1)$$

Where

$$I_c = \frac{V_{cc}+V_{ce}}{R_c} \quad (2)$$

Hence, $I_c = \frac{12-1.0}{100} = 0.11\text{A} = \mathbf{110mA}$

The base resistor ,R_b, (in Figure 6) is computed as follows;

$$V_{in} = I_bR_b + V_{be} \quad (3)$$

Hence

$$R_b = \frac{V_{in}-V_{be}}{I_b} \quad (4)$$

$$I_b = \frac{I_c}{h_{fe}} \quad (5)$$

So, $I_b = \frac{0.11}{40} = 0.00275\text{A} = 2.8\text{mA}$. Then, $R_b = \frac{12-1.0}{0.00275} = 4000\Omega = \mathbf{4K\Omega}$. The calculated values of load and base resistors are also applicable to circuit diagram in Figure 3.

2.6.2 The Transformer Unit

The step-up/step-down transformer in Figure 7 and the circuits associated with it are designed such that during the inverter mode the transformer steps up 12Vac produced by the MOSFETs switches to 220Vac and when there is the present of grid power the transformer steps down the voltage from 220Vac to 12V for charging the battery.

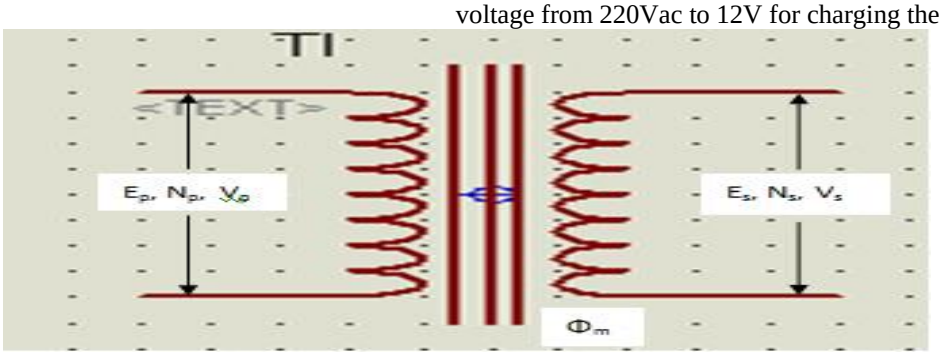

Figure 7 : The step-up/step-down transformer

(i) Inverter mode (Step-up)

The transformer key parameters are as follows;
Frequency in Hertz (Hz) (Assumed: 50Hz);
Primary e.m.f (V_P) = Input voltage = 12.6V and Secondary e.m.f (V_s) = Output voltage = 220V

Number of turns in the Primary winding ($\boldsymbol{N_P}$) and secondary winding (N_s), where N_s = 260 turns and $\boldsymbol{N_P}$ = 15.6 = **16turns** and the turn ratio, a in terms of voltage is 0.06.

2.6.3 The multi-vibrator sub-circuit

Multi-vibrator unit is the unit that generates the pulse when it is energized. It has three outputs ranging from 1 to 3 (i.e Q, $\bar{Q}$, OSC in Figure 3.8). The output frequencies of Q, $\bar{Q}$ are always twice that of output 3 (OSC). In other words, the frequency of output 3 depends on the values of capacitor C1 and resistor R1. Therefore, since 50Hz is needed across output 1 and 2, there are needed to calculate for frequency of 100Hz at output 3. However, to achieve this desirable frequency, the value of the biasing component needs to be calculated. In this case, the value of capacitor C3, is chosen while the value resistor RV8is shown in Figure 8. Other variables that need to be determined are period of oscillation (T) and duty cycle (D).

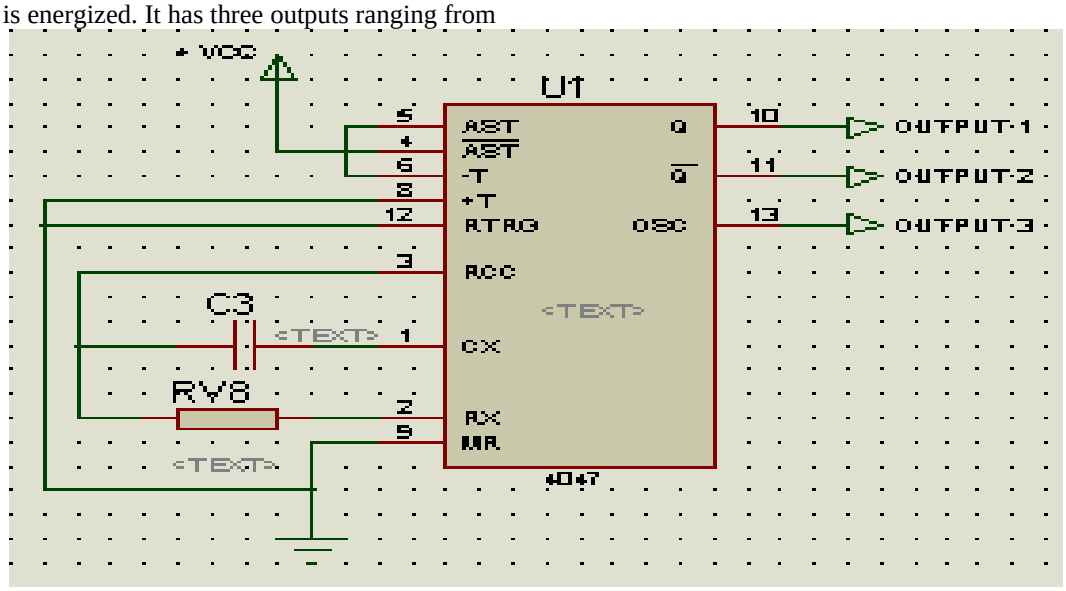

Figure 8: 4047IC sub-circuit diagram

Discharge Resistor (RV8): In Figure 8, for the 4047IC to operate in Astable mode, the frequency is given as;

$$f = \frac{1}{4.4(C3)(Rv8)} \quad (6)$$

Therefore, the values of R_{v8} is given as;

$$R_{v8} = \frac{1}{4.4(f)(C3)} \quad (7)$$

Given, C3 = 1uf and f = 50Hz , then $R_{v8} = \frac{1}{4.4\,X10^{-6}X\,50} = 4545.5\ \Omega = 4.5\text{k}\Omega$

The value of the resistor calculated is 4.5kΩ. However, a 5kΩ variable resistor is used so that during circuit construction and operation, the 5kΩ variable resistor

can be adjusted while observing with oscilloscope to achieve the required 50Hz.

Period of Oscillation (T) : The period of oscillation (T) is given as;

$$T = \frac{1}{f} \quad (8)$$

Where f = 50Hz , the $T = \frac{1}{50}$ **20msec**.

The Duty cycle (D): Duty cycle is given as;

$$D = \frac{t_{on}}{T} \times 100\% \quad (9)$$

But

$$T = t_{on} + t_{off} \quad (10)$$

Now, the 4047 IC need to generate equal pulse width, so as to stabilize the output voltage of the system, that is, $t_{on} = t_{off}$. Therefore, when T = 20msec, then T = 10msec + 10msec = 20 msec . Now, when t_{on} = 10msec then; D = $\frac{t_{on}}{T} \times 100\% = \frac{10}{20} \times 100\% =$ **50%**

2.6.4 The Comparator Sub-unit

The diagram shown in Figure 9 shows two circuit diagrams for the two comparator (U2:B and U2:C), which is extracted from the Charge Controller, High/Low Grid Voltage control Circuit in Figure 3. This device compares two input signals levels from the rectified public utility source, and switches either "On or Off" the relay. In other words, the comparators check the high/low ac voltages for a possible shutdown as the case may be. More so, in order to determine the operating voltages, the voltage divider which is used to bias the comparator in Figure 9 is first considered.

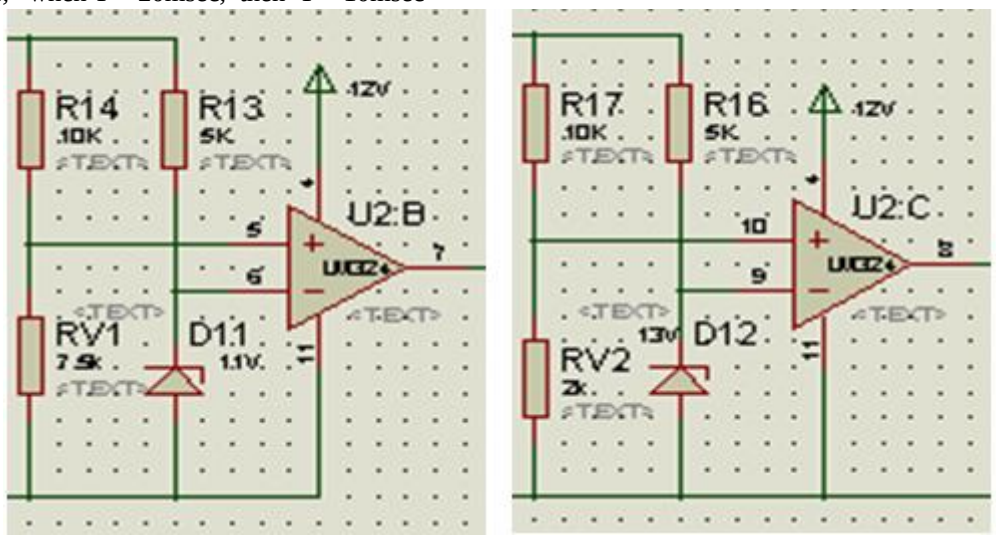

Figure 9: Comparator sub-unit extracted from the circuit in Figure 3

From Thevenin theorem ;

$$V_{out} = R_{V1}\left(\frac{V_{cc}}{R_{14}+R_{v1}}\right) \quad (11)$$

Then ;

$$R_{14} = \frac{R_{V1}\,(V_{cc})}{V_{out}} - R_{V1} \quad (12)$$

Where V_{out} = 7V, V_{cc} (High voltage unregulated) = 14V) , V_{cc} = 12V regulated, R_{V1} = 10KΩ, then, $R_{14} = \frac{10000\ X\ 14}{8} -$ 10000 = 7500Ω = 7.5KΩ.

The value of resistor R17 at low voltage shut down is given as ;

$$R_{17} = \frac{R_{V2}\,(V_{cc})}{V_{out}} - R_{V2} \quad (13)$$

Now, V_{cc} (Low voltage) = 6 V , R_{V2} = 10KΩ and V_{out} = 5V, so,

$R_{17} = \frac{10000(6)}{5}$ -10000 = 2000Ω = 2KΩ

3 Results and Discussion

3.1 System Implementation

The implementation of project was carried out in sub-sections, particularly; the various sub-sections constructed and assemble using Vero board as shown in Figure 10.

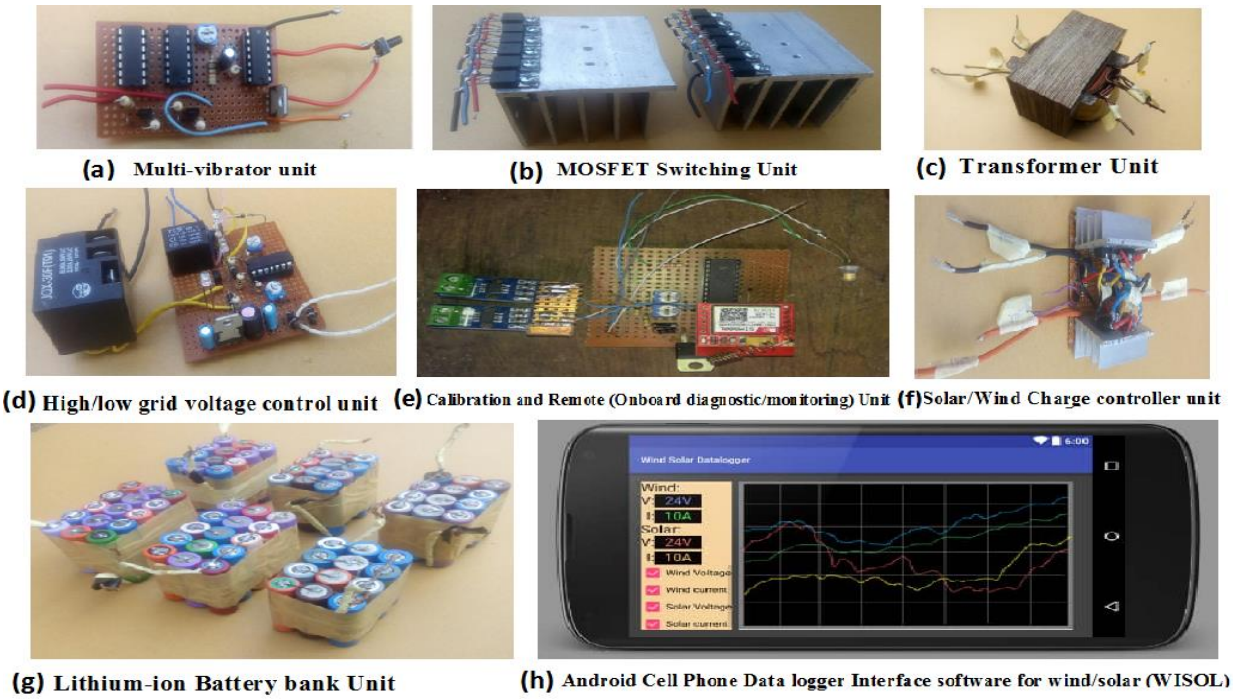

Figure 10 : **Cutout Sections of various sub-sections constructed and assemble using Vero board along with the screenshot of the android data logger interface**

The picture displayed in Figure 10 (a) is the circuit construction of multi-vibrator unit. It can be seen that three integrated circuits (4047, LM324 and 4081) are mounted on the Vero board, as well as other biasing components. They also include resistors, capacitor, transistors, voltage regulator and simulation mini switch. The construction has four wires, which serves as input and output terminals. The orange and black wires are used as input probe, while the other two red wires are for output. In other words, the multi-vibrator unit is energized with 10V dc power supply via the black and orange wires, while an output square waveform signals is obtained from the two black wires.

Consequently, Figure 10 (b) is the implemented unit of MOSFET switches fastened to the heat sink. All the twelve MOSFETs are mounted on the heat sink for quick dissipation of heat generated by the working switches. According to the image of the construction, they are two MOSTFET switches, which are constructed to operate intermittently. In this case, since they are two packs, each pack of MOSFET unit, accommodates six MOSFETs. Each pack is used to switch the weak input signal generated by multi-vibrator, and raise it amplitude to the desirable level. But in this case, the switching signals continue to remain out of phase with the other.

Figure 10(c) shows the transformer unit. The Transformer unit is developed using ferromagnetic materials, such that copper wire of a certain length is wound round the iron laminations. In this case, the six terminals are obtained. Three terminals serve as a non-inverting mode input terminals with a center tap, while the other is the output produces 13V ac for the charging of the battery bank. But during inverting mode, the initial ac input will turn output, while the other output becomes input.

Similarly, the image in Figure 10 (d) is the construction of high/low grid voltage control unit. This unit is prepared to accommodate two relay switches, resistors, LM324, capacitor and variable resistor. The white and other black wires are used for 12V ac input as well as ac (input/output) cut off supplies. Figure 10 (e) is the calibration and remote (Onboard diagnostic/monitoring) Unit. The constructed calibration and remote (onboard diagnostic/monitoring) unit consist of current sensor (blue), Wi-fi module (red), ATmega8, diodes, voltage regulator and variable resistors. All these components are mounted and soldered to the Vero board to ensure a good electrical contact. Also, in Figure 10 (f) , the construction of solar/wind charge controller unit is built and presented. This unit is built on the Vero board, such that three MOSFETs (3205) are mounted on the heat sink for easily dissipation of heat during switching (battery charging). This unit controls the charging of battery bank through photovoltaic cell and wind turbine.

The Lithium-ion battery bank unit (Figure 10(g)) which is also called a battery pack is arranged and configured to produce 12.8V/200AH. This is done through series and parallel combinations.

The Android cell phone data logger Interface software for wind/solar (WISOL) is shown in Figure 10 (h) . It displays the wind turbine and solar voltages, current and power. The display includes all input/output voltages, currents and power. It can also display the battery bank voltage level. This data logger interface accesses this information remotely and displays on the Android application. The application uses internet of things (IOT) to communicate with the inverter system, by switching either “on” or “off” any time and from any location.

3.2 Simulation based results

Figure 11 to Figure 14 is the simulated results obtained from main inverter/low battery voltage shutdown circuit diagram in Figure 2.

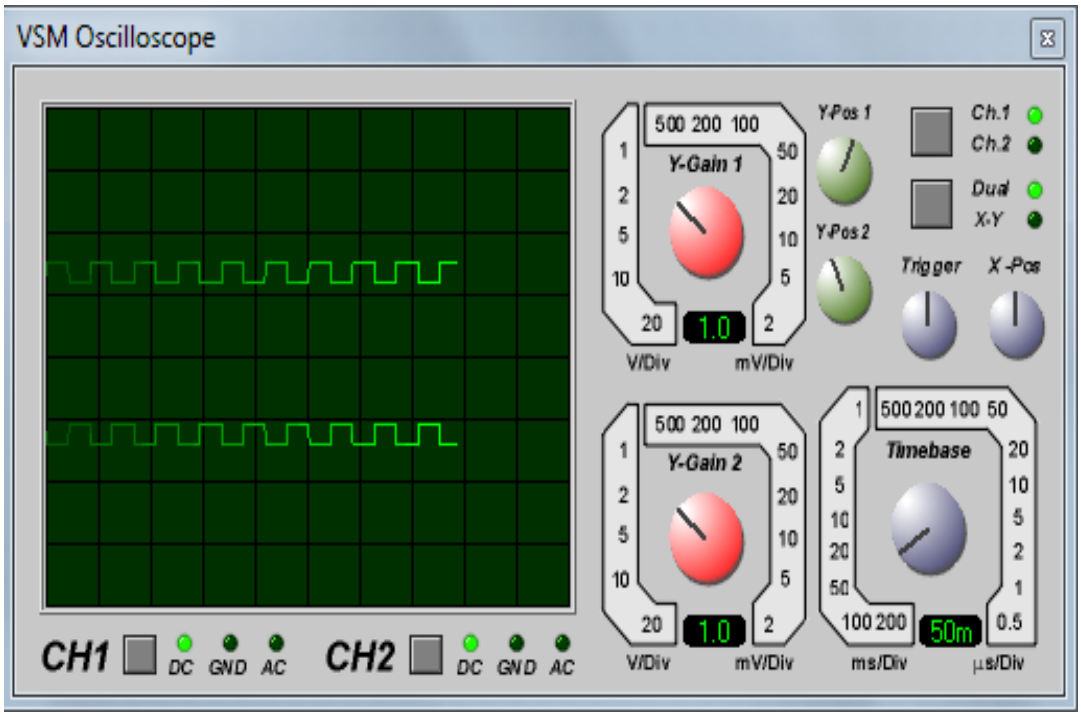

Figure 11: Output signals of 4047 integrated circuit at Q and $\bar{Q}$.

The simulation was carried out using electronic software called "Proteus". The results are obtained from three outputs of the 4047 IC, which serves as the brain of the circuit. The simulated results are captured from the source of the signal to final point in the circuit. That is, from 4047 IC signal source to the outputs of the AND gates.

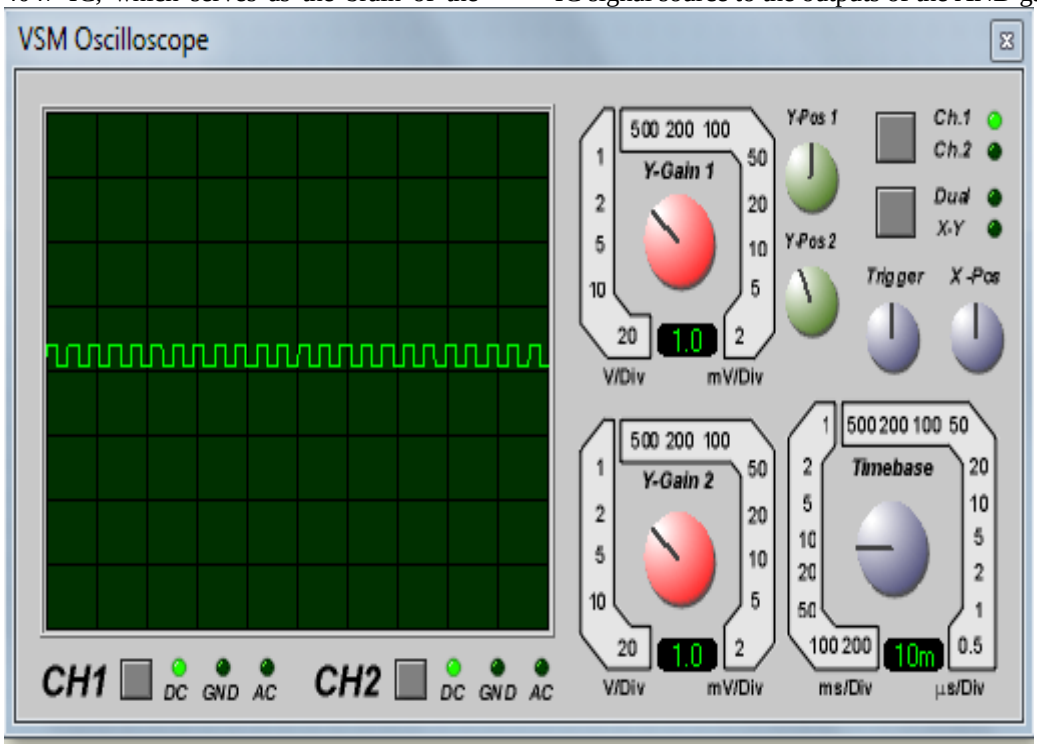

Figure 12: Output signals of 4047 Integrated circuit at pin 13.

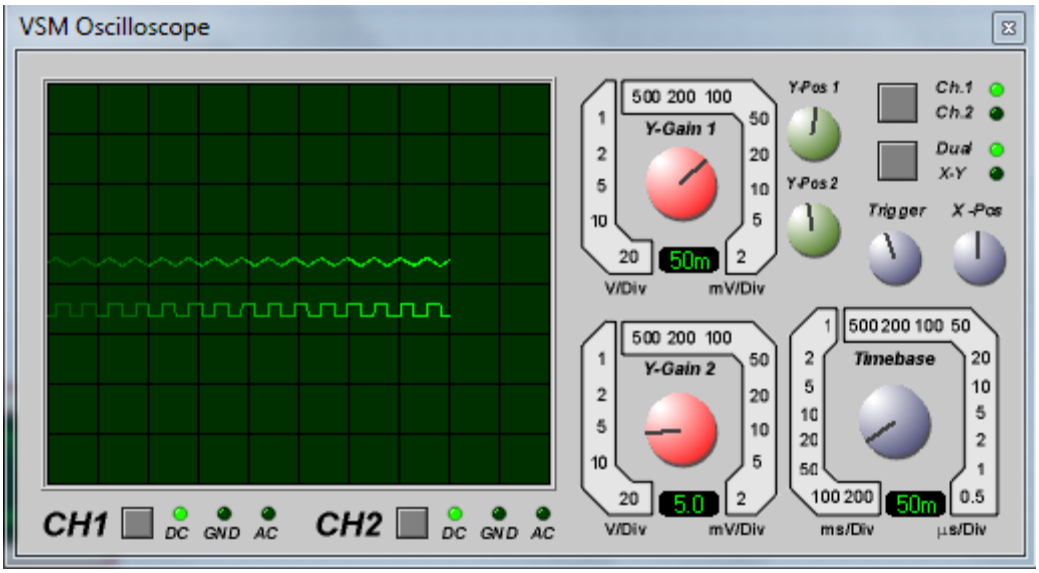

Figure 13: Output signals of high pass filter.

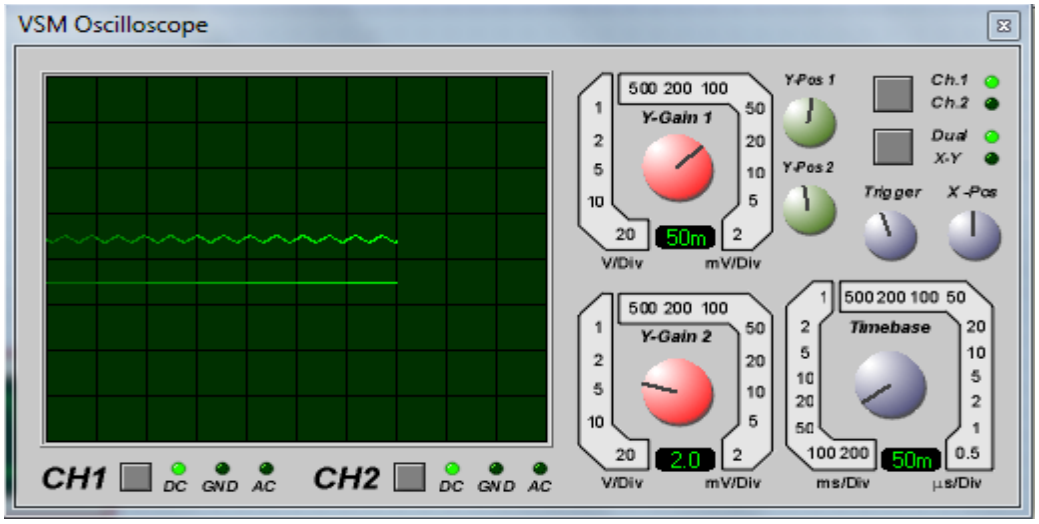

Figure 14: Inverting and non-inverting input signals of LM324 comparator

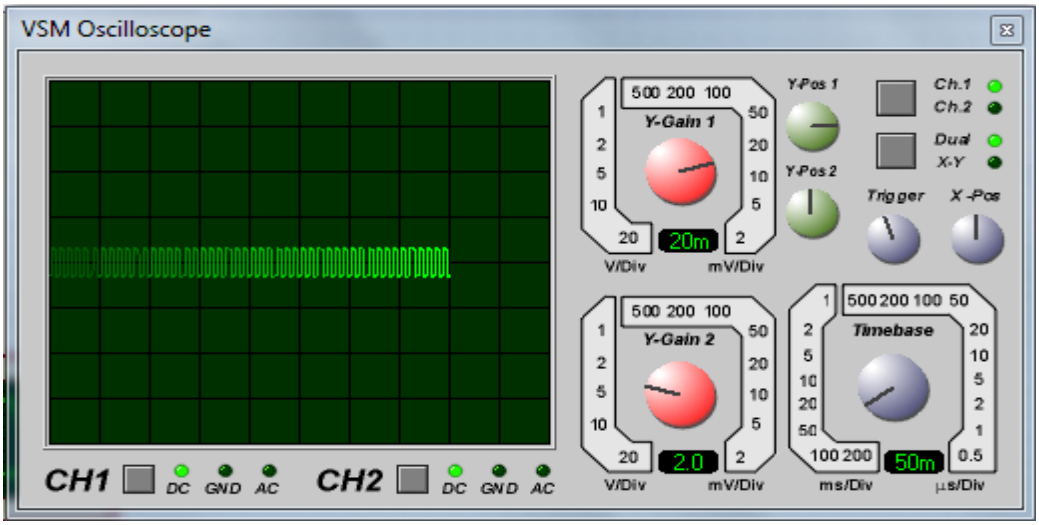

Figure 15: LM324 comparator output signal.

The diagram showed in Figure 11 is the output waveform obtained from output terminal 10 and 11 (i.e Q and $\bar{Q}$) of the 4047 IC. The 4047 IC is a multi-vibrator integrated circuit, which is considered as a signal generator in themain inverter/low battery voltage shutdown circuit diagram. Although, the 4047 IC is configured to operate at low frequency (50Hz), but since the wave nature at 50Hz is so complex and not visible, the frequency was reduced to 10Hz for proper visibility. However, the signal displayed is a square waveform in nature with equal amplitude, which oscillates in out of phase with each other. The square waveform has a gain of 1volt/division, with a propagating time-base of 50 ms/division. This is to show that the square wave signal is capable of providing successful switching signal for the conversion of dc to ac signal. It means that, the signal is used to operate the metal oxide semiconductor field effect transistors in the circuit (MOSFETs) via AND gates.

Figure 12 is simply an output result of pin 13 of 4047 IC, which is the third output terminal of the integrated circuit. The output 13 is a complementary output for pin 10 and 11, which is configured to generate a signal at the medium frequency 100Hz. According to the waveform of the signal, the square wave is twice the frequency signal compared to that of pin 10 and 11. In this case, the 100Hz signal wave is used to stabilize the main inverter system output, especially when there is a drop in the input voltage level. Also, one of the characteristics of this square wave signal is that, it has a small amplitude (10V), which can only be used low to switch or trigger bigger power devices (i.e Transistors and MOSFET).

The two signals displayed in Figure 13 is input/output waveform of the high pass filter connected to the non-inverting input of comparator U2.A in the inverter/low battery voltage shutdown circuit diagram in Figure 2. The high pass filter takes in square wave signal and converts it to a triangular waveform, which help in stabilizing the inverter output power. In this conversion, the medium frequency of 100 kHz generated by 4047 IC multi-vibrator is only allowed to pass, while other higher frequencies are blocked by the high pass filter. Therefore, the combination of triangular wave and a 12V dc which is shown in Figure 14 is compared via comparator U2.A in other to produce another square wave signal. However, this new square waveform signal is twice the output frequency signal of 4047 IC of pin 13 (i.e 200Hz). That is to say, this new square wave signal is being used to complement proper switching of the two AND gate ICs as it stabilizes the inverter overall output power.

4. Conclusion

The design, construction and simulation of the circuit for an integrated solar-wind energy system with remote monitoring and control mechanism is presented. The system block diagram is divided into six major sub-sections, namely, the solar/wind charge controller section, the inverter section, the grid connection section, the rectification section, the onboard/remote monitoring control section and the energy storage section. However, each sub-section is also made up of sub-units which provide detailed information on the components used. The circuit diagram for the sub-units were presented along with numerical examples of calculations used to determine some circuit components values. Also, the implementation of project was carried out in sub-sections, particularly; the various sub-sections were constructed and assemble using Vero board. In all, the implemented circuits were tested and the test results showed that the system functioned according to the design specifications.

References

1. Fontes, Cristiano Hora de O., and Francisco Gaudêncio M. Freires. "Sustainable and renewable energy supply chain: A system dynamics overview." *Renewable and Sustainable Energy Reviews* 82 (2018): 247-259.
2. Kumar, Nimish, and Nitai Pal. "The existence of barriers and proposed recommendations for the development of renewable energy in Indian perspective." *Environment, Development and Sustainability* (2018): 1-19.
3. Kumar, Manish, and Cherian Samuel. "Future of Renewable Distributed Generation in India." *TIDEE (TERI Information Digest on Energy & Environment)* 16.1 (2017).
4. Han, Jie, et al. "Current status of distributed energy system in China." *Renewable and Sustainable Energy Reviews* 55 (2016): 288-297.
5. Ahuja, Dilip, and Marika Tatsutani. "Sustainable energy for developing countries." *SAPI EN. S. Surveys and Perspectives Integrating Environment and Society* 2.1 (2009).
6. Foroudastan, Saeed D., and Olivia Dees. "Solar power and sustainability in developing countries." *Proceedings of the international conference on renewable energy for developing countries*. 2006.
7. Arantegui, Roberto Lacal, and Arnulf Jäger-Waldau. "Photovoltaics and wind status in the European Union after the Paris Agreement." *Renewable and Sustainable Energy Reviews* 81 (2018): 2460-2471.
8. Fan, Xiao-chao, et al. "Hybrid pluripotent coupling system with wind and photovoltaic-hydrogen energy storage and the coal chemical industry in Hami, Xinjiang." *Renewable and Sustainable Energy Reviews* 72 (2017): 950-960.
9. Benedek, József, Tihamér-Tibor Sebestyén, and Blanka Bartók. "Evaluation of renewable energy sources in peripheral areas and renewable energy-based rural development." *Renewable and Sustainable Energy Reviews* 90 (2018): 516-535.
10. Owusu, Phebe Asantewaa, and Samuel Asumadu-Sarkodie. "A review of renewable energy sources, sustainability issues and climate change mitigation." *Cogent Engineering* 3.1 (2016): 1167990.
11. He, Zheng-Xia, et al. "Factors that influence renewable energy technological innovation in china: A dynamic panel approach." *Sustainability* 10.1 (2018): 124.
12. Jacobson, Mark Z., et al. "Matching demand with supply at low cost in 139 countries among 20 world regions with 100% intermittent wind, water,

and sunlight (WWS) for all purposes." *Renewable Energy* 123 (2018): 236-248.
13. Mirjat, Nayyar Hussain, et al. "A review of energy and power planning and policies of Pakistan." *Renewable and Sustainable Energy Reviews* 79 (2017): 110-127.
14. Kabir, Ehsanul, et al. "Solar energy: Potential and future prospects." *Renewable and Sustainable Energy Reviews* 82 (2018): 894-900.
15. Nazir, Muhammad Shahzad, et al. "Environmental impact and pollution-related challenges of renewable wind energy paradigm–A review." *The Science of the total environment* 683 (2019): 436-444.
16. Jefferson, Michael. "Energy policies for sustainable development." *World Energy Assessment: Energy and the challenge of sustainability* (2000).
17. Hafner, Manfred, Simone Tagliapietra, and Lucia de Strasser. "Prospects for Renewable Energy in Africa." *Energy in Africa*. Springer, Cham, 2018. 47-75.
18. Bertoldi, P. "Guidebook: How to develop a Sustainable Energy and Climate Action Plan (SECAP)." *Publication Office of the European Union* (2018).
19. Villanueva, Arturo N., and Jennifer M. Worrall. "Establishing communication and power sharing links between components of a distributed energy system." U.S. Patent No. 9,941,696. 10 Apr. 2018.
20. Denholm, Paul, et al. *Role of energy storage with renewable electricity generation*. No. NREL/TP-6A2-47187. National Renewable Energy Lab.(NREL), Golden, CO (United States), 2010.
21. Mohamad, Farihan, et al. "Development of energy storage systems for power network reliability: A review." *Energies* 11.9 (2018): 2278.
22. Islam, M. A., et al. "Global renewable energy-based electricity generation and smart grid system for energy security." *The Scientific World Journal* 2014 (2014).
23. Villanueva, Arturo N., and Jennifer M. Worrall. "Establishing communication and power sharing links between components of a distributed energy system." U.S. Patent No. 9,941,696. 10 Apr. 2018.
24. Sanyal, Subir K. "Sustainability and renewability of geothermal power capacity." *Power Stations Using Locally Available Energy Sources: A Volume in the Encyclopedia of Sustainability Science and Technology Series, Second Edition* (2018): 47-60.
25. Martins, Florinda, et al. "Analysis of fossil fuel energy consumption and environmental impacts in European countries." *Energies* 12.6 (2019): 964.
26. Noorollahi, Younes, et al. "Modeling for diversifying electricity supply by maximizing renewable energy use in Ebino city southern Japan." *Sustainable cities and society* 34 (2017): 371-384.